GLOBAL AND SEASONAL EFFECTS OF LIGHTNING-INDUCED ELECTRON PRECIPITATION

A DISSERTATION
SUBMITTED TO THE COMMITTEE ON GRADUATE STUDIES
OF STANFORD UNIVERSITY
IN PARTIAL FULFILLMENT OF THE REQUIREMENTS
FOR THE DEGREE OF
DOCTOR OF PHILOSOPHY
IN
ELECTRICAL ENGINEERING

Austin Patrick Sousa
November 2017

I certify that I have read this dissertation and that, in my opinion, it is fully adequate in scope and quality as a dissertation for the degree of Doctor of Philosophy.

(Sigrid Close) Principal Adviser

I certify that I have read this dissertation and that, in my opinion, it is fully adequate in scope and quality as a dissertation for the degree of Doctor of Philosophy.

(Robert Marshall)

I certify that I have read this dissertation and that, in my opinion, it is fully adequate in scope and quality as a dissertation for the degree of Doctor of Philosophy.

(Antony Fraser-Smith)

Approved for the Stanford University Committee on Graduate Studies

Preface

This thesis tells you all you need to know about...

Acknowledgments

(Acknowledgements go here)

Contents

List of Tables

List of Figures

Chapter 1

Introduction

1.1 The Space Environment

1.2 Motivation

1.3 Previous Work

1.4 Thesis Organization

Chapter 2

Physics and Methods

2.1 Overview of Plasma Physics

A *plasma* is a quasi-neutral gas of ions, electrons, and neutral particles, which exhibit collective behavior. Plasmas can behave in similar ways to a conventional fluid – they can flow, they can be compressible, they can be turbulent, and so on – however the addition of charged particles facilitates many behaviors unique to a plasma. Charged particles can interact with each other not just through ballistic collisions, but at a distance through electromagnetic forces. The bulk motion of a plasma can be manipulated through electric and magnetic fields; conversely a plasma can have a substantial effect on the propagation of radio waves passing through it.

A plasma can be analyzed in several different domains: Single particle motion; fluid approximations; and full kinematic solutions. In this work we treat the motions of electrons in the single particle domain, which is a natural choice for the sparse densities and small gyroradii of radiation belt electrons. To understand the behavior of radio waves propagating through a plasma, we treat the background as a smooth dielectric medium.

2.1.1 Single Particle Motion

The high energies and sparse densities of the radiation belts lend themselves very well to a single-particle approximation. Many of the basic behaviors and quantities in plasma physics can be understood through studying the motion of a single particle.

The fundamental equation of motion for a charged particle in an electromagnetic field is given by the Lorentz force:

$$\mathbf{F} = \frac{d\mathbf{p}}{dt} = q(\mathbf{E} + \mathbf{v} \times \mathbf{B}) \tag{2.1}$$

Where q represents the particle's charge, $\mathbf{E}$ and $\mathbf{B}$ represent the electric and magnetic fields, and $\mathbf{v}$ the particle's velocity, shown here in a non-relativistic frame.

Electric fields simply apply a force in the direction of the field. However, note that a cross product is perpendicular to both terms – therefore any forces induced by the magnetic field will be perpendicular to the particle's velocity. The magnetic field is a *conservative* force, in that a stationary magnetic field cannot directly impart energy into a particle, but can alter a particle's trajectory. The particle will therefore have a net drift in the direction of the electric field, while exhibiting a helical motion around the magnetic field.

We can then split the velocity vector into two quantities – $v_{\parallel}$ parallel to the magnetic field, and $v_{\perp}$ perpendicular to the magnetic field.

Two characteristic values arise from this motion: the radius of the particle's rotation around the magnetic field, known as the *gyroradius* or the *Larmor radius*:

$$r_l = \frac{mv_{\perp}}{qB} \tag{2.2}$$

And the rotation frequency, known as the *gyrofrequency* or *cyclotron frequency*:

$$\omega_c = \frac{v_{\perp}}{r_l} = \frac{qB}{m} \quad [\text{rad/sec}] \tag{2.3}$$

By integrating the particle's momentum over a single gyrorotation, we arrive at a third fundamental quantity known as the magnetic moment, or the *first adiabatic*

invariant:

$$\mu = \frac{mv_\perp^2}{2B} \tag{2.4}$$

In situations where the magnetic field varies slowly (e.g., on spatial scales much greater than the gyroradius), then μ remains a constant of motion.

A final parameter to describe a particle's motion is it's *pitch angle*, the angle between the velocities perpendicular and parallel to the magnetic field:

$$\alpha = \tan^{-1}\left(\frac{v_\perp}{v_\parallel}\right) \tag{2.5}$$

The first adiabatic invariant describes an implicit relationship between the magnetic field strength and a particle's pitch angle at a given point. Combining the first adiabatic invariant with conservation of kinetic energy, we can deduce an expression for magnetic trapping – that is, the magnetic field strength in which a particle exhibiting helical motion along a magnetic field line will turn around at.

$$E = \frac{1}{2}mv^2 \tag{2.6}$$

$$= \frac{1}{2}m(v_\parallel^2 + v_\perp^2) \tag{2.7}$$

$$= \frac{1}{2}mv^2(\cos^2\alpha + \sin^2\alpha) \tag{2.8}$$

At a reflection point, the particle's kinetic energy will be entirely in the perpendicular mode:

$$\frac{v_{\perp 0}^2}{B_0} = \frac{v_{\perp 1}^2}{B_1} \tag{2.9}$$

$$\frac{v^2\sin^2(\alpha)}{B_0} = \frac{v^2}{B_1} \tag{2.10}$$

$$\sin^2(\alpha) = \frac{B_0}{B_1} \tag{2.11}$$

Therefore, a charged particle in a magnetic field will be constrained to rotate around a field line, and bounce back and forth, reflecting where the magnetic field strength increases. A key takeaway is that the reflection point is independent of

energy, and depends only on the ratio of magnetic field strengths and the particle's initial pitch angle. An example of this behavior is shown in figure 2.1.

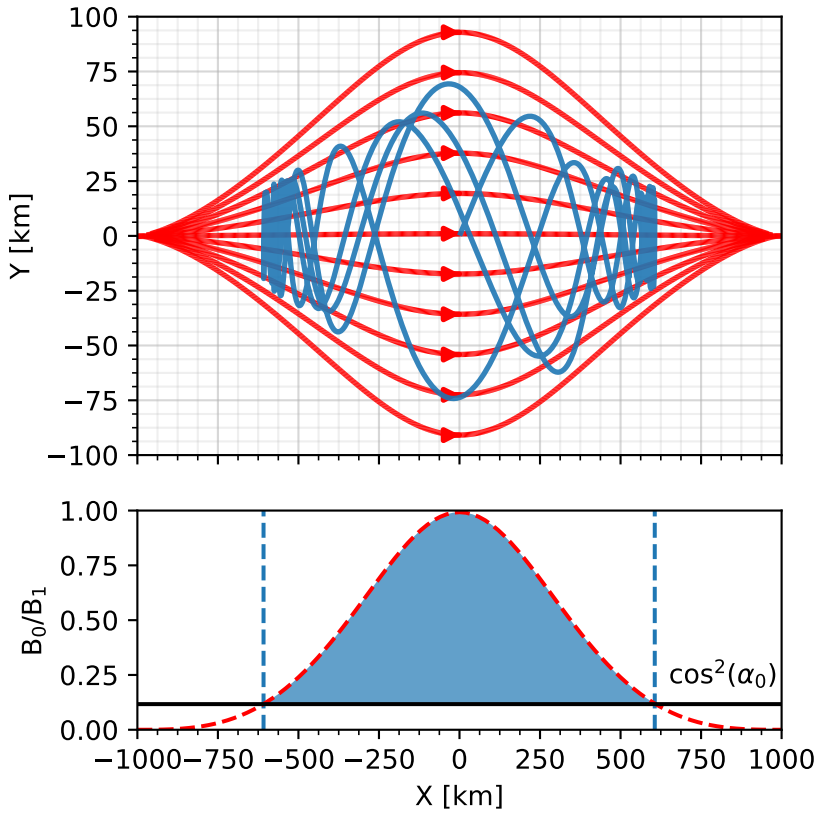

Figure 2.1: An example of a "magnetic bottle" particle trap. The top plot shows the trajectory of an electron with an initial pitch angle $\alpha_0 = 20°$. The bottom plot shows the magnetic field ratio B_0/B_1, with the particle's reflection points shown as vertical lines.

2.1.2 Waves in Plasmas

Previously, we have described the motion of a charged particle under the influence of an electromagnetic field. the single-particle approximation provides enormous insight into the dynamics of a sparsely-populated plasma. Next, we must consider the inverse

system – how the charged particles in a plasma dictate the characteristic behaviors of an electromagnetic wave propagating through it.

An electromagnetic wave can accelerate a charged particle; conversely, an accelerating or decelerating particle induces its own electromagnetic field. It would seem, then, that the behavior of an electromagnetic field in a plasma is simply the summation of the contributions of each particle and some incident wave source. However, the complexity of this brute-force approach quickly becomes intractable for even a handful of particles. The universal approach taken then is to abstract the complicated interplay of waves and particles into a wave moving through a dielectric medium, described only by the various constituent densities, temperatures, and background field intensities within a given volume.

As with any electromagnetic problem, we begin with Maxwell's equations – shown here in their non-relativistic, differential form, in SI units:

$$\nabla \cdot \mathbf{E} = \frac{\rho}{\epsilon_0} \tag{2.12}$$

$$\nabla \cdot \mathbf{B} = 0 \tag{2.13}$$

$$\nabla \times \mathbf{E} = -\frac{\partial \mathbf{B}}{\partial t} \tag{2.14}$$

$$\nabla \times \mathbf{B} = \mu_0 \mathbf{J} + \frac{1}{c^2}\frac{\partial \mathbf{E}}{\partial t} \tag{2.15}$$

$\mathbf{E}$ and $\mathbf{B}$ denote the electric and magnetic fields; μ_0 and ϵ_0 denote the magnetic permeability and electric permittivity of free space; and $c = \sqrt{\frac{1}{\mu_0 \epsilon_0}}$ is the speed of light. The terms ρ and $\mathbf{J}$ represent the local charge density and current density, both of which may be functions of position and time.

By taking the curl of equation 2.14 and substituting in the time derivative of equation 2.15, and making use of the vector identity $\nabla \times \nabla \times \mathbf{E} = \nabla(\nabla \cdot \mathbf{E}) - \nabla^2 \mathbf{E}$, we have:

$$\nabla^2 \mathbf{E} - \frac{\nabla \rho}{\epsilon_0} = \mu_0 \frac{\partial \mathbf{J}}{\partial t} + \frac{1}{c^2}\frac{\partial^2 \mathbf{E}}{\partial t^2} \tag{2.16}$$

In the absence of charges or currents ($\rho = 0$, $\partial \mathbf{J}/\partial t = 0$), the equation reduces to

the free-space wave equation:

$$\nabla^2 \mathbf{E} = \frac{1}{c^2} \frac{\partial^2 \mathbf{E}}{\partial t^2} \tag{2.17}$$

Next, we linearize the system and search for harmonic perturbations of the form:

$$\mathbf{E}(\mathbf{r}, \mathbf{t}) = \mathbf{E_1} e^{i(\omega t - \mathbf{k} \cdot \mathbf{r})} \tag{2.18}$$

$$\mathbf{B}(\mathbf{r}, \mathbf{t}) = \mathbf{B_0} + \mathbf{B_1} e^{i(\omega t - \mathbf{k} \cdot \mathbf{r})} \tag{2.19}$$

$$\mathbf{J}(\mathbf{r}, \mathbf{t}) = \mathbf{J_1} e^{i(\omega t - \mathbf{k} \cdot \mathbf{r})} \tag{2.20}$$

where ω is the wave angular frequency, $\mathbf{k}$ is the wave vector, or spatial frequency, and $\mathbf{r}$ is the spatial coordinate. Two fundamental parameters of an electromagnetic wave are the *phase velocity*, ω/k, and the *group velocity*, $\partial\omega/\partial k$. The relation between the temporal and spatial frequencies is known as the *dispersion relation*.

From here we follow the derivation and convention used by *Stix* (1992) and *Bittencourt* (2004). In general, a plasma is comprised of several different species of constituent particles – positively and negatively charged particles necessary to maintain a quasi-neutral plasma. While the dispersion relations of different species cannot be simply added, their effects can be summed to form the displacement current $\mathbf{J}$:

$$\mathbf{J} = \sum_s \mathbf{J_s} = \sum_s n_s q_s \mathbf{u_s} \tag{2.21}$$

where n, q, and $\mathbf{u}$ represent the (number) density, charge, and velocity of a particular species s.

We make the assumption that the plasma is *cold* – that is, that the velocities of each species $\mathbf{u_s}$ have a single value each. Were we to relax this assumption, each species density would have a distribution function in both position and momentum, $n = n(\mathbf{r}, \mathbf{p})$; the total current would then be an integration over momentum for each species. For a treatment of a hot plasma, see the work by *Sazhin* (1993).

Next, we note that, in a cold plasma assumption, the Lorentz force (equation 2.1)

can be written for each species:

$$m_s \frac{d\mathbf{u_s}}{dt} = q_s\big(\mathbf{E} + \mathbf{u_s} \times \mathbf{B}\big) \tag{2.22}$$

Combining equations 2.18 – 2.20, 2.21, and 2.22, and assuming a coordinate system with the background magnetic field $\mathbf{B_0}$ aligned with the z-axis, we arrive at an expression for the *cold-plasma dielectric tensor*:

$$\boldsymbol{\epsilon} \cdot \mathbf{E} = \begin{pmatrix} S & -iD & 0 \\ iD & S & 0 \\ 0 & 0 & P \end{pmatrix} \begin{pmatrix} E_x \\ E_y \\ E_z \end{pmatrix} \tag{2.23}$$

The various summations over each constituent species are incorporated into the so-called Stix parameters (*Stix* (1992)):

$$S = \frac{1}{2}(R + L) \qquad D = \frac{1}{2}(R - L) \tag{2.24}$$

$$R = 1 - \sum_s \frac{\omega_{ps}^2}{\omega(\omega + \omega_{cs})}; \quad L = 1 - \sum_s \frac{\omega_{ps}^2}{\omega(\omega - \omega_{cs})}; \quad P = 1 - \sum_s \frac{\omega_{ps}^2}{\omega^2} \tag{2.25}$$

where $\omega_{ps} = n_s q_s^2/\epsilon_0 m_s$ and $\omega_{cs} = q_s B_0/m_s$ are the plasma and cyclotron frequencies for species s.

Dispersion Relation

With the dielectric tensor now determined, we can derive the relationship between ω and $\mathbf{k}$, known as the dispersion relation. Equation 2.16 can be written as:

$$\boldsymbol{\eta} \times \boldsymbol{\eta} \times \mathbf{E} + \boldsymbol{\epsilon} \cdot \mathbf{E} = 0 \tag{2.26}$$

where $\boldsymbol{\eta} = \mathbf{k}c/\omega$ is the wave refractive index. Assuming a wave propagating with some angle θ between $\boldsymbol{\eta}$ and the background magnetic field, we arrive at:

$$\begin{pmatrix} S - \eta^2 \cos^2\theta & -iD & \eta^2 \cos\theta \sin\theta \\ iD & S - \eta^2 & 0 \\ \eta^2 \cos\theta \sin\theta & 0 & P - \eta^2 \sin^2\theta \end{pmatrix} \begin{pmatrix} E_x \\ E_y \\ E_z \end{pmatrix} = 0 \tag{2.27}$$

Taking the determinant of 2.27 yields the *cold-plasma dispersion relation*:

$$A\eta^4 - B\eta^2 + C = 0 \tag{2.28}$$

$$A = S\sin^2\theta + P\cos^2\theta \tag{2.29}$$

$$B = RL\sin^2\theta + PS(1 + \cos^2\theta) \tag{2.30}$$

$$C = PRL \tag{2.31}$$

Equation 2.28 is biquadratic – we can solve for $\eta^2 = k^2c^2/\omega^2$ using the quadratic formula.

Finally, it is worth noting that when considering a single-species plasma (e.g., electrons only), equation 2.28 reduces to the well-known *Appleton-Hartree Equation* (*Appleton* (1932)):

$$\eta^2 = 1 - \frac{\frac{\omega_{pe}^2}{\omega^2}}{1 - \frac{\omega_{ce}^2 \sin^2\theta}{2(\omega^2 - \omega_{pe}^2)} \pm \left[\left(\frac{\omega_{ce}^2 \sin^2\theta}{2(\omega^2 - \omega_{pe}^2)}\right)^2 + \frac{\omega_{ce}^2}{\omega^2}\cos^2\theta\right]^{1/2}} \tag{2.32}$$

The dispersion relation in equation 2.28 reveals a wealth of information about the characteristics of waves in plasmas. For various plasma densities and background magnetic field strength, we can infer which wave frequencies may propagate, if any, and which wave polarizations. Through the remainder of this work, we will be concerned with the *Whistler* mode – a right-hand, circularly-polarized (RHCP) wave. Within a typical magnetospheric plasma, the Whistler mode spans the VLF band, roughly between 30 Hz and 300 kHz.

Figure 2.2 shows a typical dispersion relation for a magnetospheric plasma (L $\approx$

2) by plotting frequency vs wavenumber ($\eta = kc/\omega$). The Whistler mode is the lower branch of the RHCP mode.

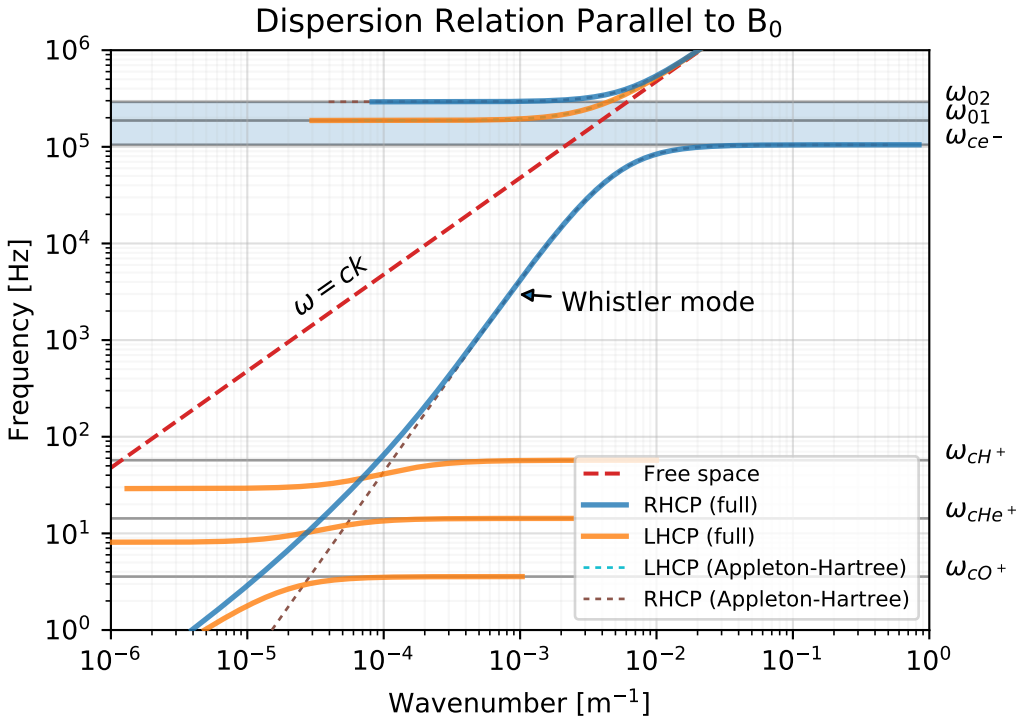

Figure 2.2: An ω-K diagram for the cold plasma dispersion relation, shown here for a wave propagating parallel to $\mathbf{B}$, in four-component plasma with $N_e \approx 6 \times 10^8\, e^-/m^3$, and $B \approx 4\,\mu T$. For higher frequencies the dispersion relation asymptotes to the free-space solution, with slope c. The Whistler mode is the right-hand, circularly-polarized mode which spans the majority of the frequency band. The shaded region marks the characteristic band in which the right-hand mode cannot propagate. At lower frequencies, the left-hand circular mode resonates with the various ion constituents, known as the *Ion Cyclotron* modes.

2.2 Ray Tracing and Landau Damping

2.2.1 Ray Tracing

Whistler-mode waves in the magnetosphere propagate for very large distances, and with relatively little attenuation. Under certain conditions, these waves can persist from a few seconds to 1 or more minutes. Simulating the propagation of these waves using a full-wave method would be extremely intractable with current computational resources. However we can use ray tracing to approximate their behavior.

Ray tracing is a technique from geometric optics which tracks the position and velocity of a coherent wave packet – essentially, approximate the behavior of a wave packet to that of a photon, and evaluate the packet's velocity and wavenormal vector with respect to time. Ray tracing is best suited for coherent, monochromatic wave packets, with no attenuation, dispersion, or mode coupling.

Ray tracing was first applied to the Whistler mode by *Haselgrove* (1954) using a graphical technique, and by *Haselgrove and Haselgrove* (1960) and *Kimura* (1966) for numerical computation. These papers worked in curvilinear coordinates with respect to a magnetic field line. Haselgrove's Equations have been used extensively by numerous magnetospheric scientists (*Kimura*, 1966; *Edgar*, 1972; *Ngo*, 1989; *Jasna Ljiljane Ristic-Djurovic*, 1993; *Lauben*, 1998; *B.Peter*, 2007; *Bortnik*, 2005; *Kulkarni*, 2009), several using the so-called "Stanford Ray Tracing Program" – a legacy Fortran code which evaluated the Haselgrove equations in two dimensions. Our work uses a slightly different code originally developed by Dr. Forrest Foust (*Golden et al.*, 2010), and is designed for flexibility with respect plasma density and magnetic field models. Rather than work in curvilinear coordinates with explicit derivatives, we adopt a more-general formulation, using a three-dimensional Cartesian frame and numerically-evaluated derivatives.

We begin with the fundamental ray-tracing equations, as given by *Haselgrove and Haselgrove* (1960); *Stix* (1992):

$$\frac{d\mathbf{r}}{dt} = \frac{\nabla_k F}{\partial F/\partial \omega} \tag{2.33}$$

$$\frac{d\mathbf{k}}{dt} = \frac{\nabla_r F}{\partial F/\partial \omega} \tag{2.34}$$

$$\tag{2.35}$$

Constrained such that:

$$F = F(\mathbf{r}, t, \mathbf{k}, \omega) = 0 \tag{2.36}$$

Equation 2.33 is simply $\frac{\nabla_k F}{\partial F/\partial \omega} \approx \frac{\partial F/\partial k}{\partial F/\partial \omega} = \frac{\partial \omega}{\partial k} = V_g$, the group velocity of a wave packet. The corresponding equation describing the evolution of the wavenormal vector (2.34) is less intuitive, although an analogy can be drawn to Hamiltonian mechanics, in which ω represents a velocity, and k a momentum.

The function F, our "conserved quantity", is simply the cold plasma dispersion relation given by equation 2.28.

The raytracing equations are a set of coupled, first-order differential equations; solutions to which require some subtlety, but can be addressed using standard numerical techniques.

First, note that we can solve the set at a given time, then evolve the system forward some finite time step. However, the constraint $F = 0$ may not be strictly held afterward. We assert that the error in this constraint must be small; which in turn implies that the background medium must be smoothly-varying – i.e., changing on a spatial scale much greater than our forward step, and of the wavelength of interest. This assumption is known as the *WKB Approximation.*

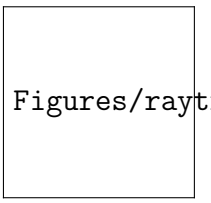

Figure 2.3: Example ray tracing

Adaptive Timestepping

The process of raytracing, then, is to 1) solve the dispersion relation (2.28) to find the refractive index; 2) compute the velocity vector and step the system forward in time; and 3) re-evaluate at the new position to assure that the condition F=0 remains held. However, properly selecting the timestep is of critical importance – too large a timestep and positional errors will accumulate, or the ray will slip out of a propagating mode; too small and computational speed and memory usage suffers. We use an adaptive *Runge-Kutta-Fehlberg* (RK45) (*Fehlberg*, 1969; *John H. Mathews*, 2004) method to continuously update the timestep as the raytracer progresses. RK45 is a common technique for solving ordinary differential equations.

The RK45 method approximates a solution with an initial stepsize dt using two spline fits: a fourth-order and a fifth-order. The error in the step is taken to be the difference between the two estimates. If the error is above a specified tolerance ϵ, the stepsize is reduced and the evaluation is repeated. Additionally, if the error is below a specified tolerance ($\epsilon/10$ in our implementation), the stepsize is increased. The result is a variable time axis with finer resolution in regions of high variability, while enabling longer timesteps in smooth regions for computational efficiency.

2.2.2 Landau Damping

The cold-plasma formulation of raytracing described above evaluates the trajectory and wavenormal angle of a wave packet – however, it assumes zero attenuation of wave energy. While it is possible to account for wave attenuation in ray tracing using warm plasma corrections (*Sazhin*, 1993; *Henyey*, 1980), we follow the same approximation as used in the legacy ray tracing code, and calculate attenuation along the cold-plasma raypath according to Landau damping.

Landau damping, originating in a seminal work by *Landau* (1946), is a resonant interaction between a wave and the distribution of electrons and ions comprising the background medium. The Landau mechanism is an interaction with parallel streaming particles and the wave's electric field. Resonant particles are accelerated or decelerated by the wave's electric field; if a majority of the resonant electrons have

velocities slightly below that of the wave, then a coherent effect exists, the wavefront imparts some net energy to the plasma, and the wave is attenuated. Conversely, if the majority of resonant particles are moving faster than the wave, some of their energy can be imparted to the wavefront, inducing *wave growth* (*Chen*, 1983; *Kulkarni*, 2009).

Landau damping can have multiple resonances (in which the particle has multiple complete rotations per rotation of the wave). The lowest resonant mode is known as the *Landau* resonance, while the ± 1 modes are referred to as the *Cyclotron* resonances. Higher-order modes remain nameless.

We use the expressions for Landau damping as formulated by *Brinca* (1972). *Brinca* derived expressions for Landau damping assuming a cold background plasma with a sparse warm distribution added, for Whistler waves propagating at an arbitrary angle to the background magnetic field. Inputs to this formulation are the familiar Stix parameters (equations 2.24 - 2.25), which are in turn a function only of location and wave frequency; the wavenormal angle with respect to the background magnetic field; and a distribution function which specifies the energies (and thus velocities) of thermal electrons.

Interestingly, *Brinca*'s work was motivated by measurements of Whistler-mode wave growth, rather than attenuation. Our implementation follows suit, and is equally capable of returning growth or damping, depending on the plasma model used. However, throughout this research, wave growth has been exceedingly rare.

Thermal electron distributions

2.3 Coordinate Systems

In dealing with any geographic system, one will almost surely run into difficulty with coordinate systems. Most research fields make use of different coordinate systems which better-suit the minutia of their work. Since LEP is a large-scale coupling process which spans several different regions of the Earth and Space Environment, it is useful to discuss the coordinate systems we will use, and the processes of mapping from frame to frame. For an in-depth review of many additional coordinate systems,

see the work by *Laundal and Richmond* (2016).

Geographic and Geodetic coordinates

Magnetic Dipole coordinates

Earth Centered, Earth Fixed (ECEF)

Solar Magnetic

Mapping vector quantities between polar and Cartesian frames

2.4 Lightning Illumination Model

A single lightning flash is a stochastic dielectric breakdown process. While a terrestrial lightning flash consists of several repeated strokes at varying incident angles, we adopt the simplified model used by *Lauben* 1998, *Bortnik* 2005, and subsequent workers.

The lightning flash is modeled as a single, vertical current pulse from a height H_E, with a time profile given by equation 2.37:

$$I(t) = I_0(e^{-at} - e^{-bt}) \tag{2.37}$$

We relate the time-domain current profile to radiated power using the far-field approximation for an arbitrary source, given by *Griffiths* (1999), page 457:

$$S(t) \approx \frac{1}{\mu_0}(\mathbf{E} \times \mathbf{B}) = \frac{\mu_0}{16\pi^2 c}\left[\ddot{p}(t)\right]^2 \left(\frac{\sin^2\theta}{r^2}\right)\hat{\mathbf{r}} \tag{2.38}$$

where $p(t)$ is the dipole moment given by $p = 2H_E \int_0^t I(t)dt$, r is the distance from the flash in meters, and θ is the angle to the flash. Taking the second derivative of the dipole moment (the first derivative of the current profile) gives us the far-field time-domain power equation:

$$S(t) = \frac{1}{Z_0}\left(\frac{\mu_0 H_E I_0}{2\pi}\right)^2 \left(\frac{\sin^2\theta}{r^2}\right)\left(ae^{-at} - be^{-bt}\right)^2 \hat{\mathbf{r}} \tag{2.39}$$

where we have used the relation $Z_0 = \mu_0 c$. Equation 2.39 has units of energy flux density, Watts per square meter (J/m^2/sec).

To determine the frequency spectrum of the radiated power, we take the Fourier transform of equation 2.39:

$$S(\omega) = \frac{1}{Z_0}\left(\frac{\mu_0 H_E I_0}{2\pi}\right)^2 \left(\frac{\sin^2\theta}{r^2}\right)\frac{\omega^2(a-b)^2}{(\omega^2+a^2)(\omega^2+b^2)}\hat{\mathbf{r}} \tag{2.40}$$

which has units of energy flux per frequency – J/m^2/Hz.

Throughout this work we assume a flash height H_E=5 km, and model parameters $a = 5 \times 10^3\,\mathrm{sec}^{-1}$ and $b = 1 \times 10^5\,\mathrm{sec}^{-1}$, resulting in a spectrum peaked at approximately 4kHz; any lightning flash can be parameterized solely by its peak current I_0 and its location on the surface of the Earth. Figure 2.4 shows the current profile and associated spectrum.

2.5 Trans-Ionosphere Attenuation

2.6 Wave-Particle Interactions

2.7 Environment Models

Within this work, we will encounter several different regions of the space environment – This section provides a collected overview of each region and the models used.

2.7.1 Magnetic Field

Magnetic Dipole

IGRF

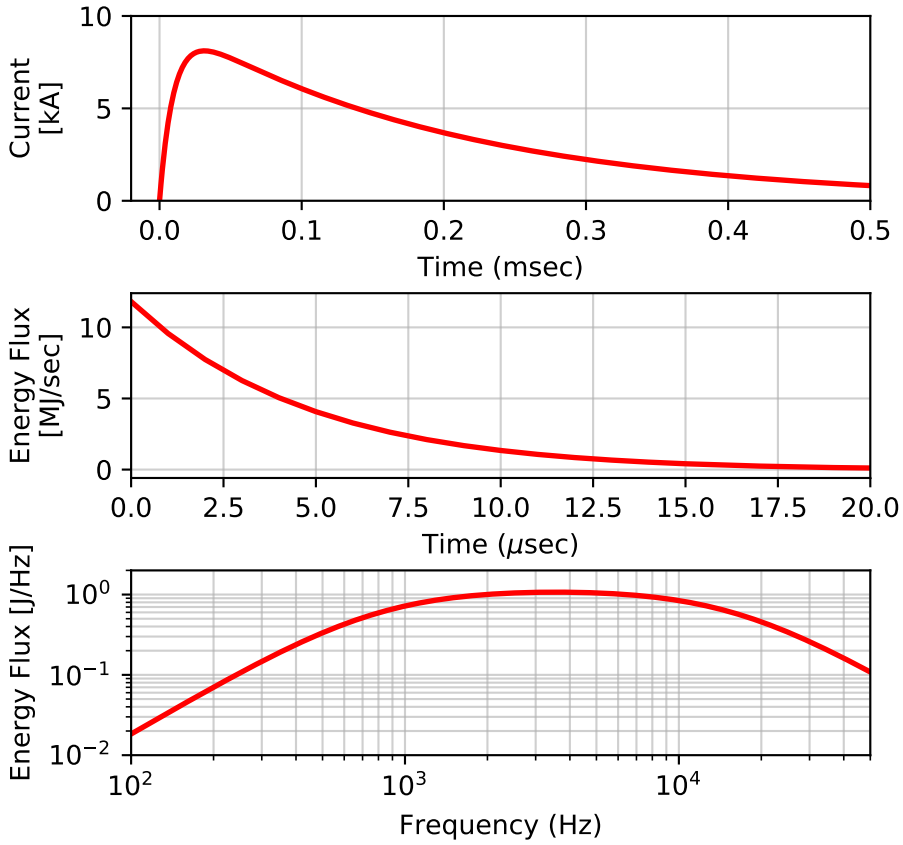

Figure 2.4: Double-exponential current pulse model of a lightning stroke. The top panel shows the stroke current vs time; the middle panel shows the total energy flux, integrated over space, vs time; the bottom panel shows the energy flux in the frequency domain.

Tsyganenko Corrections

2.7.2 Ionosphere

IRI

2.7.3 Plasmasphere

The plasmasphere is a region of the space environment surrounding the Earth, and a primary unknown within our modeling. The plasmasphere extends from an altitude of 1000km up to several Earth radii; typically it is divided into two separate regions: a dense, relatively cold *inner plasmasphere*, and a sparse, relatively hot *outer plasmasphere* or *trough*. The transition boundary between the two regions is a sharp dropoff in plasma density called the *plasmapause*.

Much like the ionosphere, the plasmasphere is a highly variable region, depending on solar conditions (K_p), location (latitude, longitude, field line), and time of day (MLT). The large spatial scales, high variability, and sparse availability of in-situ measurements require us to turn to empirical models of each region. We consider three primary models of electron density, and two of electron temperature.

Overview of Plasmasphere Density Models

Ngo Model The Ngo model is a legacy model used extensively in research at Stanford from the early 1980s through the mid-2000s, notably by *Lauben* (1998) and *Bortnik* (2005), and has heritage dating back to the early days of radioscience at Stanford (*Kimura*, 1966) The model uses a Diffusive Equilibrium (DE) model for the inner and outer plasmasphere, onto which the *Carpenter and Anderson* (1992) inner plasmasphere model is overlaid. This model was integrated into the legacy Stanford VLF raytracing code, and provided several adjustable parameters, including plasmapause location, constituent ratios, and the ability to include ducts.

Global Core Plasmasphere Model The Global Core Plasmasphere Model (GCPM), initially developed in 2000 by *Gallagher et al.* (1999) with significant updates through

the following decade, smoothly transitions between several regional models to provide a continuous model of the plasmasphere. Within this work we use version 2.4, which was released in 2009 and made available by the Space Plasma Physics group at the NASA Marshall Space Flight Center (https://plasmasphere.nasa.gov). GCPM incorporates the *Carpenter and Anderson* (1992) inner plasmasphere model and the *Gallagher et al.* (1995) outer plasmasphere model, with an empirical fit of the plasmapause location between. The polar cap model is derived from *Persoon et al.* (1983) and *Chandler et al.* (1991). All models are connected smoothly to the IRI model of the ionosphere at lower altitudes. The combined GCPM model is parameterized by K_p and MLT.

Simplified GCPM GCPM aims to provide a dynamic, complete picture of the plasmasphere as a function of time and K_p; however for our purposes GCPM provides too much variation. Additionally, the combination and smoothing between many models is computationally slow. In order to provide quicker computation and to reduce the number of parameters to adjust, we have implemented a simplified version of GCPM.

This model uses the equatorial-plane GCPM model, including the plasmapause location. However we omit any variation along latitude, and assume densities are constant along each field line. As our region of interest lies primarily within low and mid latitudes, we omit the polar cap model altogether and simply merge the ionosphere into the equatorial trough model. Finally to simplify computation, we model the ionosphere using an empirical fit to IRI – one for noon, and one for midnight, with a smooth transition along longitude.

Figure 2.5 shows a side-by-side comparison of the three models.

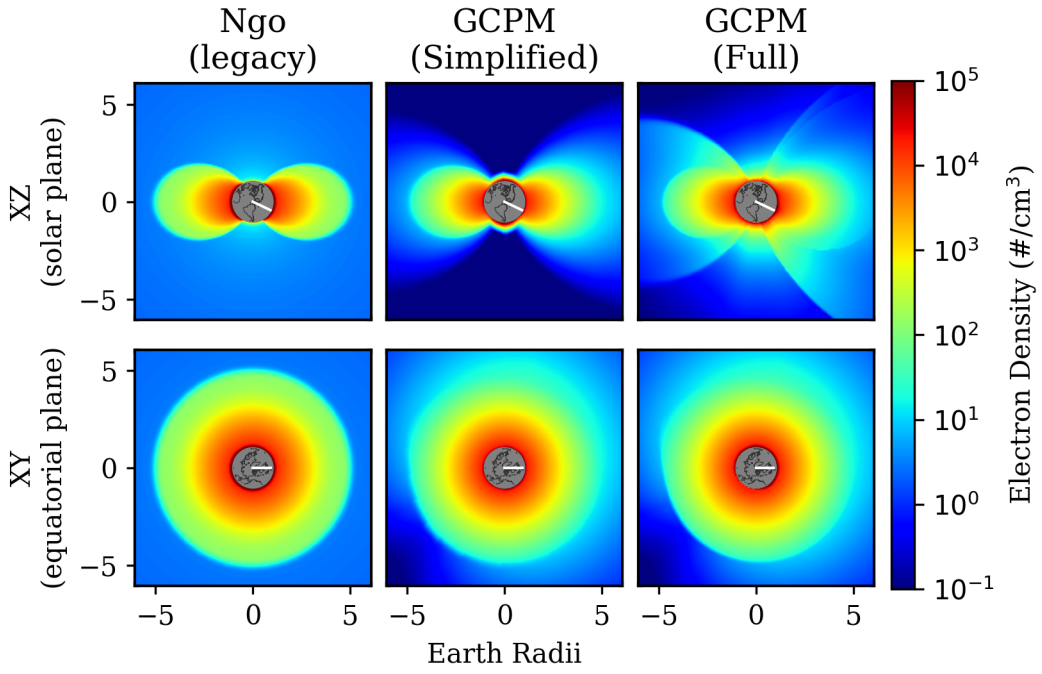

Figure 2.5: A comparison of three plasmasphere models: Ngo, simplified GCPM, and full GCPM, for a relatively quiet plasmasphere ($K_p = 2$). The top row shows electron density in-plane with the direction of solar influx; the bottom row shows a top down (equatorial cross-section) view. The white line indicates the solar axis. Only electron density is shown, as additional plasma constituents are derived from electron density.

Chapter 3

VLF energy in the Near-Earth Environment

The purpose of this chapter is to provide a quantifiable assessment of the persistent radio wave energy in the near-Earth space environment due to lightning-generated Whistlers.

3.1 Overview of Previous Work

3.2 Methodology

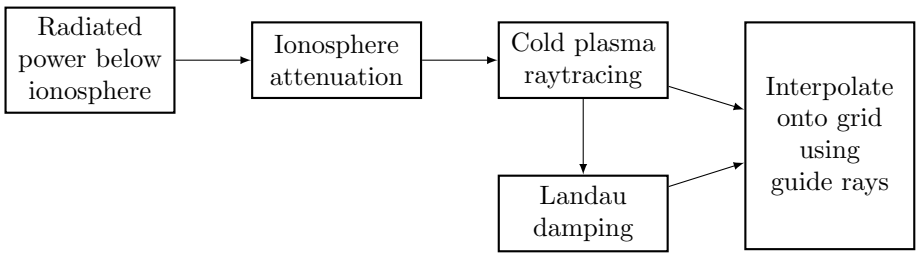

Figure 3.1: Block diagram

3.2.1 Gridding and Interpolation

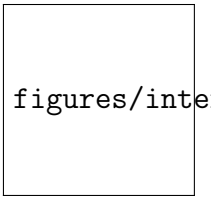

Figure 3.2: Interpolation scheme

3.2.2 Persistent Energy from a Single Flash

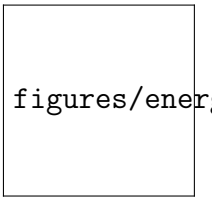

Figure 3.3: Block diagram

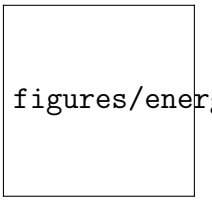

Figure 3.4: Block diagram

3.2.3 Global Energy Density

Chapter 4

3D Modeling of LEP

4.1 Overview of Previous Work

Pseudo-3D vs Scaled 2D

Geometric Factor

Chapter 5

Global and Seasonal Estimates of LEP

5.1 Overview of Previous Work

Where should you put the magnetosphere statistics? that big correlation plot of kp, ae, Dst, etc etc

Chapter 6

Satellite Instrumentation for LEP Measurement

6.1 VPM Mission Overview

6.2 Hardware Architecture

6.2.1 Wave Measurement

6.2.2 Particle Measurement

6.3 Firmware Architecture

Chapter 7

Conclusions

Bibliography

Appleton, E. V. (1932), Appleton : Wireless Studies of the Ionosphere . Wireless Studies of the Ionosphere .* Appleton : Wireless Studies of the Ionosphere ., (10).

Bittencourt, J. A. (2004), *Fundamentals of Plasma Physics*, 3rd ed.

Bortnik, J. (2005), Precipitation of radiation belt electrons by lightning-generated magnetospherically reflecting whistlers, *Stanford University Thesis*, (January), 1–199.

B.Peter, W. (2007), Quantitative Measurement of Lightning-Induced Electron Precipitation Using Vlf Remote Sensing, (February).

Brinca, A. L. (1972), On the Stability of Obliquely Propagating Whistlers, *Journal of Geophysical Research*, *77*(19), 3495–3507.

Carpenter, D. L., and R. R. Anderson (1992), An ISEE / Whistler Model of Equatorial Electron Density in the Magneto sphere Od D ' j :, *J. Geophys. Res.*, *97*, 1097–1108.

Chandler, O., M. O. Chandler, J. H. Waite, and T. E. Moore (1991), Observations of polar ion outflows, *Journal of Geophysical Research: Space Physics*, *96*(A2), 1421–1428, doi:10.1029/90JA02180.

Chen, F. F. (1983), *Introduction to Plasma Physics and Controlled Fusion*, Plenum PRess, New York, NY, doi:QC718.C39 1983.

Edgar, B. (1972), The structure of the magnetosphere as deduced from magnetospherically reflected whistlers, Ph.D. thesis, Stanford University.

Fehlberg, E. (1969), Low-order classical Runge-Kutta formulas with stepsize control and their application to some heat transfer problems, *Tech. Rep. July*, NASA.

Gallagher, D. L., P. D. Craven, R. H. Comfort, and T. E. Moore (1995), On the azimuthal variation of core plasma in the equatorial magnetosphere, *Journal of Geophysical Research: Space Physics*, *100*(A12), 23,597–23,605, doi: 10.1029/95JA02100.

Gallagher, D. L., P. D. Craven, and R. H. Comfort (1999), Global Core Plasma Model, *Journal of Geophysical Research: Space Physics*, *105*(A8), 18,819–18,833, doi:10.1029/1999JA000241.

Golden, D. I., M. Spasojevic, F. R. Foust, N. G. Lehtinen, N. P. Meredith, and U. S. Inan (2010), Role of the plasmapause in dictating the ground accessibility of ELF/VLF chorus, *Journal of Geophysical Research: Space Physics*, *115*(11), 1–15, doi:10.1029/2010JA015955.

Griffiths, D. J. (1999), *Introduction to Electrodynamics*, 3rd ed., Prentice-Hall, Inc, Upper Saddle River, New Jersey.

Haselgrove, J. (1954), Ray theory and a new method for ray tracing, *Report of the Physical Society Conference on Physics of the Ionosphere*, pp. 355–364.

Haselgrove, J., and C. B. Haselgrove (1960), Twisted ray paths in the ionosphere, *Proceedings of the Physical Society*, *75*, 357–363, doi:10.1088/0370-1301/70/7/302.

Henyey, F. S. (1980), Improved ray description of wave equations, *Physical Review Letters*, *45*(24), 1897–1900, doi:10.1103/PhysRevLett.45.1897.

Jasna Ljiljane Ristic-Djurovic (1993), Gyroresonant Scattering of Radiation Belt Electrons by Oblique Whistler Waves, Ph.D. thesis, Stanford University.

John H. Mathews, K. K. F. (2004), *Numerical Methods Using Matlab*.

Kimura, I. (1966), Effects of Ions on Whistler-Mode Ray Tracing, *Radio Science*, *1*(3), 269–283, doi:10.1002/rds196613269.

Kulkarni, P. (2009), Controlled precipitation of radiation belt electrons, Ph.D. thesis, Stanford University, doi:10.1029/2002JA009580.

Landau, L. D. (1946), On the vibrations of the electronic plasma, *Soviet Journal of Physics*.

Lauben, D. (1998), Precipitation of Radiation Belt Electrons by Obliquely-Propagating Lightning-Generated Whistler Waves, Ph.D. thesis, Stanford University.

Laundal, K. M., and A. D. Richmond (2016), Magnetic Coordinate Systems, *Space Science Reviews*, pp. 1–33, doi:10.1007/s11214-016-0275-y.

Ngo, H. D. (1989), Electrostatic waves stimulated by VLF whistler mode waves scattering from magnetic-field-aligned plasma density irregularities, Ph.D. thesis, Stanford University.

Persoon, A. M., D. A. Gurnett, and S. D. Shawhan (1983), Polar cap electron densities from DE 1 plasma wave observations, *Journal of Geophysical Research: Space Physics*, *88*(A12), 10,123–10,136, doi:10.1029/JA088iA12p10123.

Sazhin, S. (1993), *Whistler-mode Waves in a Hot Plasma*, 1 ed., Cambridge University Press, Cambridge.

Stix, T. H. (1992), *Waves in Plasmas*, American Institute of Physics, New York, NY, doi:QC718.5.W3S75.